

Future changes in winter wind-climate over Europe

H.W. van den Brink, B.J.J.M. van den Hurk

February 2, 2007

Contents

1. Introduction	2
2. Methodology	3
3. Model validation	3
a. winter-mean MSLP climatology	3
b. Winter-mean wind climatology	4
c. Comparison of high wind speeds in RCMs with GCM	4
4. Greenhouse gas induced changes in MSLP and wind	5
a. Greenhouse gas effects on NH MSLP	5
b. CO ₂ effects on NA wind speed	5
c. Change of distribution of local annual maximum wind	6
5. Construction of the climate scenarios for wind speed in The Netherlands	6
6. Does the number of storms increase?	7
7. Discussion and Conclusions	8

Abstract

Here we present the climate change signals for the daily mean wind speed, for spatial and temporal scales ranging from the Northern Hemisphere down to once-per-year exceeded local quantities in the Northeast Atlantic region.

Four state-of-the-art General Circulation Models (GCMs), used for the IPCC Fourth Assessment report (AR4) do not indicate an increase of the extreme winds speeds averaged over the Northern Hemisphere due to enhanced greenhouse gas concentrations, although there are considerable spatial differences. Three of the four analyzed models show similar changes in mean sea level pressure (MSLP) patterns over the North-Eastern Atlantic and European region in winter, resulting in a more zonal flow over Western Europe. This enhanced zonality is accompanied by once-per-year exceeded wind speeds that are several percents higher. The fourth model shows neither an increase in zonal flow over Western Europe, nor an increase in the annual extreme winds.

For the once-per-year extremes of the extra-tropical daily-mean winds in winter, the GCM results are as good as high-resolution Regional Climate Models (RCMs) nested in their domains. This justifies a direct use of the GCM output for studies for e.g. safety design levels and climate change signals.

Using MSLP as a proxy for the number and intensity of extra-tropical storms may not be useful to assess climate change impacts on storm intensity, as more extreme MSLP do not necessarily correspond with increases in storm intensity.

The climate scenarios for the once-per-year exceeded daily mean wind speed, constructed for The Netherlands for 2050 range from -1% to 4%. This indicates that the impact of climate change on these wind extremes is small.

1. Introduction

After extensive scientific research of the effects of increased greenhouse gas concentrations on (spatial and temporal) averaged values of meteorological quantities, the focus is shifting to changes in the statistics of weather extremes on regional or local scale. Besides changes in temperature and precipitation, an important issue is the question whether the storm climate changes or not. Although the determination of a robust signal in wind climate is hard to find (both due to the large variability of the wind climate, and due to the rather indirect relation between elevated greenhouse gas concentrations and wind), an important motivation for investigating changes in wind extremes is the large impact of these extremes on society, for instance floodings of low-lying countries like The Netherlands due to storm surges.

Current state-of-the-art GCMs are more and more realistic in simulating synoptic-scale weather systems. This has led to an increased interest in the results of the GCMs for wind climatology, with special attention for the wind extremes. Recently, several studies have addressed the topic of changing wind extremes both on hemispheric scale (e.g. *Lambert and Fyfe* 2006; *Bengtsson et al.* 2006) and regional scale (e.g. *Leckebusch et al.* 2006). Also implications, for example concerning wind energy (*Pryor et al.* 2005) are addressed. Although the studies agree in some aspects such as the poleward shift of the storm track (*Yin* 2005), they differ in the answer to the question whether the strength and number of extra-tropical cyclones increases or not (e.g. *Leckebusch et al.* (2006) and *Lambert and Fyfe* (2006)) or not (e.g. *Bengtsson et al.* 2006).

In this paper, we give an overview of the changes in mean and extreme winds according to the SRESA1B scenarios of four state-of-the-art IPCC AR4 models for the Northern Hemisphere and the

Northeast Atlantic, and address the question whether the extratropical storm climate changes (according to these models) or not.

2. Methodology

As a starting point for our analysis, we took the models selected by *van Ulden and van Oldenborgh* (2006) (UvO hereafter). The selection was guided by the models' ability to simulate the climatological monthly-mean mean sea level pressure (MSLP) patterns of the 1960-2000 climate on both global and regional scale. Their analysis resulted in selection of the models CCCMA, MPI-ECHAM, GFDL and MIROC-HI (UvO also selected the UKMO-HadGEM1 model, but no daily data was available for this model). The resolution and time slices of the models used are given in Table 1. In our analyses, we compare the the SRESA1B scenarios with the control (20C3M) scenario. The model data are obtained via the archive of the Program for Climate Model Diagnosis and Intercomparison (PCMDI). Daily-mean wind data that are available from the PCMDI archive are listed in Table 2.

We make the basic assumption that the change in wind extremes scales linearly with the global mean temperature change. This assumption will be explained later in this paper. As Figure 1 shows, the global mean temperature more or less stabilizes for the SRESA1B scenario after 2100 (except for the MIROC-HI model). This stabilization allows to combine the daily sets after 2080 (listed in Table 2) in order to increase the record length, and thus to reduce statistical noise.

In this study, we start the analysis for the large-scale hemispheric winter-mean (Oct-Mar) MSLP patterns, then focus on the winter-mean and once-per-year exceeded daily-mean wind speed on the European regional scale, and conclude with an analysis of change in the probability density function of the once-per-year exceeded daily-mean wind speed for the North Sea. The latter analysis is relevant for the storm surge in The Netherlands, and thus the design heights of the sea dikes.

This once-per-year exceeded wind speed is represented by the location parameter of the so-called Gumbel distribution, which is fitted to the annual maxima of the squared wind speed (see e.g. *van den Brink et al.* 2004).

3. Model validation

In line of the aims of this paper, we first compare the Northern Hemisphere winter-mean pressure at sea level (MSLP) model fields with the ERA40 fields. The output of the models is interpolated to the 2.5° grid of the ERA40 dataset.

Second, we verify the wind extremes in winter for the North-Atlantic and European region. Finally, in order to examine if Regional Climate Models (RCMs) do systematically improve the statistics of extreme winds or not, we compare the extreme wind speeds from (RCMs) with those from GCMs.

a. winter-mean MSLP climatology

Figure 2 shows the seasonal mean MSLP pattern in the ERA40 data set over the 1960-2000 period for the Northern Hemisphere winter (O-M). Also the difference of each model with respect to the ERA40 data set is shown. All these models show a reasonable representation of the observed MSLP patterns over the Northern Hemisphere (see also UvO), although the position of the North Atlantic storm track is slightly too southerly (especially in the GFDL model) and the Pacific storm track is (considerably) too deep in the CCCMA and MIROC-HI models. All the models show too high MSLP values around 20°N and too low values around 50°, and (to a lesser extend) too high MSLP around the North Pole.

b. Winter-mean wind climatology

Figure 3 shows the winter-mean (O-M) wind speed for ERA40 dataset over the 1960-2000 period for the North-Atlantic and European region, and the difference of each GCM with ERA40. All models produce reasonable winter-mean wind speeds, generally within 1 m/s of the ERA40 winds. Larger differences are mainly caused by differences in (resolution dependent) orography. CCCMA produces too high wind speeds over land; all models produce satisfactory winds over sea. Note that, according to *Caires and Sterl* (2003), the ERA40 system slightly underestimates high wind speeds over sea (see also <http://www.knmi.nl/onderzk/oceano/waves/era40/era40.html>). The biases in MSLP patterns (Figure 2) do not result in wrong positions of high-wind areas (in Figure 3).

c. Comparison of high wind speeds in RCMs with GCM

For regional phenomena, Regional Climate Models (RCMs) are often used, as they have a higher spatial and temporal resolution than GCMs. This results in a better resolution of gradients induced by land-sea boundaries, sea surface temperatures (SSTs) and orography.

In order to find possible differences in statistics of (extreme winter) wind speeds, we intercompare the extreme winds obtained from GCM and RCM output and observations.

Figure 4 shows the return level plots of the annual maximum wind speeds for a set of RCMs, all driven by the same GCM (as part of the PRUDENCE project, *Christensen and Christensen* 2006), for the grid points nearest to the location of the K13 oil-platform (3.2E,53.2N). Also the observations at this location are shown. The observed wind records are homogenized and transformed to potential wind (i.e. transformed to a 'standard' roughness and height) by *Verkaik* (2000).

The figure shows that, for the annual wind speed maxima, the annual wind speed maxima of the different RCMs fluctuate around the distribution of the driving GCM. The average of the five fits to the RCMs is virtually identical to the fit of the driving GCM. Apparently, an arbitrary RCM does not systematically generate higher winds than its driving GCM.

The slopes of the GCM- and RCM-curves (representing the relation between increase of intensity and decrease of frequency) are more or less similar to that of the ERA40 curve. From this fact we conclude that the models behave realistically with respect to the underlying mechanism that determines the frequency of extreme cyclones.

Note the considerable offset between the observed data and the ERA40 data, which may indicate the underestimation of the high wind speeds by the ERA40 system, as mentioned before (*Caires and Sterl* 2003).

The same conclusion i.e., that the intensity-frequency relation of extreme cyclones of GCMs is similar to that of RCMs, can be drawn from Figure 5, which shows the cross-section of once-per-year minimum MSLP averaged between 25°W and 10°W for two RCM simulations with different boundary conditions. Again, the RCM does not generate deeper depressions than the driving GCM; they follow the climate of the GCMs, resulting in statistically similar behavior as their driving GCM.

Apparently, this similarity between GCM- and RCM wind and MSLP extremes only holds for the winter season. In summer, the wind extremes are often originating from small-scale systems, which are better resolved by RCMs than by GCMs.

The similarity for the wind climate in winter may be further explained by the fact that the stronger jet stream in winter reduces the residence time of the cyclones within the RCM domain. A possible extra deepening potential of the RCM cannot be realized within the short time of the cyclone within the RCM domain. This result differs from the findings of *Jung et al.* (2006), who finds a strong relation between the deepening of extra-tropical cyclones and horizontal resolution. This paradox may be caused by the fact that the West Atlantic region, where cyclones are generated, is not incorporated in

the domain of the RCMs, in contrast to *Jung et al.* (2006).

We conclude that RCMs do not give additional information on the variable of interest here, and we proceed with the analysis of GCM results

4. Greenhouse gas induced changes in MSLP and wind

The effects of increased greenhouse gas concentrations on wind-related quantities is analyzed for three different spatial and temporal scales. First, changes in hemispheric flow patterns are analyzed by means of the winter-mean (Oct-Mar) MSLP. Second, winter-mean and once-per-year exceeded (O-M) wind speed is analyzed for the North-Atlantic and European region. Third, changes of the probability distribution of annual extremes on a local scale are discussed. In addition, the construction of the wind scenarios for The Netherlands are discussed (*van den Hurk et al* 2006). We conclude with a discussion about the apparent paradox in literature about changes in mid-latitude storm frequency and intensity.

a. Greenhouse gas effects on NH MSLP

Comparisons of the winter-mean (Oct-Mar) and annual minimum MSLP between the 20C3M and SRESA1B scenarios are shown in Figure 6 and 7 respectively.

All models react with a (zonally averaged) decreased MSLP at high latitudes ($> 60^\circ\text{N}$), and (to a lesser extend) increased MSLP at 30° , indicating an enhanced zonal flow.

In the GFDL model, the North-Atlantic storm-track extends further to the North-East. This model, together with the MPI-ECHAM model (and to a lesser extend the CCCMA model), shows in the SRESA1B scenarios a more zonal flow over Western Europe (around 50°N). The MIROC-HI model shows more zonality at higher latitudes, around 65°N .

All models show a shift of the Pacific storm-track: North-Eastward for the CCCMA and the MPI-ECHAM model, and Northward for the GFDL and the MIROC-HI model (see also *Yin* 2005).

The effect on the once-per-year exceeded daily-mean MSLP shows the same features as the winter-mean changes: a decrease of the once-per-year MSLP minima at high latitudes, and a (smaller) increase at 30°N (Figure 7). The amplitude of the change in the once-per-year signal is similar to the winter-mean signal, which implies a shift in the probability distribution without a change in shape.

b. CO_2 effects on NA wind speed

The greenhouse gas effects of the SRESA1B scenario on the winter-mean and annual maximum wind patterns for the North-Atlantic and European area are shown in Figure 8 and 9 respectively.

The North-Eastward shift/elongation of the North-Atlantic storm-track in GFDL and MPI-ECHAM5, presented in Figure 6, corresponds with an increase of the winter-mean wind speed of 5 to 10% over central Europe. The same effect is visible in the once-per-year exceeded wind speed (left panels in Figure 8), although the relative increase is slightly less ($\approx 5\%$).

The GFDL models shows unrealistic behavior in the wind-difference pattern over Europe, which is not present in the MSLP pattern (Figure 6). Over Germany and Russia it shows areas with unrealistically strong decreases in wind speeds embedded in a increasing environment.

The CCCMA model shows a slight decrease in the mean wind speed in the NA storm track, and a strong increase over central Europe and over the North Pole. Remarkably, the increase over land is only present in the winter-mean, and not in the extreme wind speeds.

The MIROC-HI model does not show a change in wind climate over the NA ocean nor over Western Europe. Similar to the CCCMA model, strong increase in winter-mean and annual maximum wind speeds is apparent over North America in this model.

The zonally averaged change in annual extreme wind and MSLP is shown in Figure 10. It shows that the sign of the climate change of once-per-year exceeded wind speed and MSLP are strongly meridionally dependent. For instance, all models show lower winds at 30°N, and higher winds at 70°N.

c. Change of distribution of local annual maximum wind

Although the models show some large-scale similarities in the changes in the wind climate, they differ considerably at the local scale. For instance, the GFDL and the MPI-ECHAM5 models indicate a clear increase of winter-mean- and annual maximum wind speed over Western Europe (around 50°N), whereas in CCCMA this is much less clear, MIROC-HI does not show this increase at all.

For the change in distribution of the annual maximum wind speed, we focus on the North Sea, taking the grid point nearest to (2.5°E,55°N) as a reference.

Figure 11 shows a return level plot of the annual maximum wind speeds for the ERA40 dataset and of the four models, for both scenarios. It reveals a systematic bias between the ERA40 and the 20C3M scenario in the distribution of annual maximum wind speed over the North Sea, for all models. However, as mentioned before, the similar slopes of the fits suggests that the GCMs realistically represent the mechanism that determines the frequency of intense cyclones. Reminding that the ERA40 data are possibly too low (Figure 4 and *Caires and Sterl (2003)*), this implies that information about the change in the extreme wind speed derived from the GCMs may still be valuable.

The SRESA1B scenarios show a constant increase in extreme winds for all return periods, varying from ≈ 0.4 m/s for the the MIROC-HI model to ≈ 1.5 m/s for the MPI-ECHAM model. These results confirm that the change is better described by a shift than a scaling of the (extreme) wind speed.

5. Construction of the climate scenarios for wind speed in The Netherlands

The construction of the climate change scenarios for The Netherlands are described by *van den Hurk et al (2006)*. The starting point is to relate meteorological changes to changes of two steering parameters. The first parameter is the estimated global mean temperature change in 2050: a so-called G scenario of 1°C increase relative to 1990, and a W scenario of 2°C global mean temperature rise respectively. The second steering parameter is whether the change in atmospheric circulation over Central Europe is small or large. This results in four scenarios: G,G+,W and W+.

In accordance with Figure 6, MPI-ECHAM5, GFDL and CCCMA represent the regime with an enhanced zonal flow (the + scenarios), whereas MIROC-HI represents the scenarios with small changes in zonal flow.

In our analysis, we assume a linear relation between the change in wind speed and global temperature increase. Although the sampling uncertainty is large, Figure 12 shows that this assumption is fair for the reference grid point (2.5°E,55°N).

The spatial variation within the (0-10°E;50-60°N) area was used to estimate the uncertainty in the estimated change in once-per-year exceeded wind speed. This process is visualized in Figure 13, which shows the histograms of the relative changes of the once-per-year wind speed from all grid points within the (0-10°E;50-60°N) area, grouped into the two circulation scenarios. Here, the

relative wind speed changes were linearly scaled to a global temperature increase of 2°C. Figure 13 shows that the W scenario (containing MIROC-HI) shows a change in annual wind extremes that is not more than 1%. The models representing the W+ scenario show an increase in the range from -1% to 6% (neglecting the outliers of GFDL), with an average of 2%.

In order to span the whole range of probable wind changes, the 10% and 90% percentiles are attributed to the W and W+ scenarios respectively, resulting in values of -1% for the W scenario, and 4% for the W+ scenario. Using the assumption that the change in wind speed scales with the global temperature change, the values for the G and G+ scenarios are set to half of the W and W+ scenario values (rounded to full percents), resulting in 0% and 2% respectively.

6. Does the number of storms increase?

There is still a debate whether or not the number of storms and their intensity will increase due to increased greenhouse gas concentration. For instance, *Lambert and Fyfe (2006)* report that almost all models used for the IPCC Fourth Assessment Report (4AR) exhibit a significant increase of the number of extreme storms (defined as MSLP < 970 hPa). They hypothesize that the decrease of the total number of storms identified by a local minimum in MSLP is related to enhanced atmospheric stability, due to elevated heat transport amount by the extreme cyclones.

Also *Leckebusch et al. (2006)*, driving multiple RCMs with different GCMs, report an increase of the number of extreme storms for the European region.

On the other hand, e.g. *Bengtsson et al. (2006)*, who use an advanced storm tracking algorithm, do not detect an increase in the number of extreme storms in the MPI-ECHAM5 model, whereas this model shows, according to the *Lambert and Fyfe (2006)*-criterion, one of the strongest increases of extreme storms, i.e. 15% in 2100.

To solve this paradox, the following considerations should be taken into account. First, *Lambert and Fyfe (2006)* mix two criteria: for the counting of the number of storms a gradient is used (i.e. a relative measure), whereas an absolute measure (a fixed threshold) is used to determine the intense storms. A decrease in mean background MSLP will influence the counting of the number of intense storms, but not or hardly the counting of the total number of storms.

A second consideration is illustrated by Figure 10, which gives the zonally averaged change in annual extreme wind and MSLP. The fact that the sign of the climate change of once-per-year exceeded wind speed and MSLP are strongly meridionally dependent, implies that the change in storm intensity depends on the region that is considered. Third, as mentioned by *Bengtsson et al. (2006)*, one should be careful in interpreting MSLP changes in terms of effects on storm frequency and intensity. For instance, at 60°N (the latitude with lowest MSLP values, Figure 10), all models combine a 2 hPa decrease in once-per-year MSLP minima (resulting in more counts for extreme storms in the *Lambert and Fyfe (2006)*-analysis) with no or only small changes in once-per-year wind speed maxima. The same conclusion can be drawn from Figure 14, which shows that a shift to more extreme (region-averaged) MSLP can coincide with less extreme wind speed.

We conclude with the following statements. First, zonally averaged changes in extreme wind speeds are small (< 3% between 60°S and 60°N). Second, the changes are hardly statistically significant. Third, interpretation of changes of MSLP may not be useful to assess climate change impacts on storm intensity.

7. Discussion and Conclusions

We used the daily-averaged wind and MSLP fields of CCCMA, MPI-ECHAM, GFDL and MIROC-HI in order to investigate the change in extreme wind speed in the SRESA1B scenario with respect to the 20C3M scenario. The selected GCMs adequately reproduce the current global and European monthly MSLP patterns. The GCM wind fields are directly used, and not dynamically downscaled by RCMs, as the RCMs do not systematically change the daily mean extreme winds compared to the driving GCM.

All four GCMs reveal a zonally averaged decrease of MSLP for latitudes north of 50°N, and all but CCCMA an increase of the MSLP at 30°N. However, this higher meridional pressure gradient of approx. 5 hPa (model-averaged) does not result in intenser cyclones, as the model-averaged once-per-year wind speed between 30°N and 70°N does not change.

On European scale, the CCCMA, MPI-ECHAM and GFDL show a stronger zonality over Western Europe. For the MPI-ECHAM and GFDL models, this results in wind extremes that are about 1 m/s higher for all return periods around 55°N.

The MIROC-HI models does not show a strong increase of zonal flow. For this reason, the climate scenarios for The Netherlands use this model for a different scenario than obtained from the other GCMs. Combination of these sets with two possibilities of global temperature change in 2050 (G=1°C; W=2°C) results in four possible scenarios, for which the projected increase of the once-per-year wind speed varies between -1 and 4%.

In view of the year-to-year variability of the wind climate, this practically means that the range of projected climate changes falls within the uncertainty of estimated return values for return periods larger than 10 years. Combined with the considerable bias in the distribution of extreme winds of the GCMs, it is hard to make any firm statement about changes in extreme wind behavior with the current knowledge. For this reason, the probable changes in extreme wind speeds, presented in the climate scenarios, should only serve as a range of probable outcomes. Nevertheless, this range may be useful for sensitivity studies, for instance for dike design criteria. Using the (extreme) MSLP as a proxy for cyclone frequency and intensity may be misleading, and is thus not encouraged. We suggest the use of the GCM generated 10m-wind (or related quantities as the relative vorticity at 850 hPa) for storm analysis, instead of MSLP.

References

- Bengtsson, L.B., K.I. Hodges, and E. Roeckner (2006), Storm tracks and climate change, *Journal of Climate*, 19(15), 3518–3543, doi:10.1175/JCLI3815.1.
- Caires, S., and A. Sterl (2003), Validation of ocean wind and wave data using triple collocation., *J. Geophys. Res.*, 108(C3, 3098), doi:10.1029/2002JC001491.
- Christensen, J.H., and O.B. Christensen (2006), A summary of the prudence model projections of changes in the european climate by the end of this century., *Climatic Change*, in press.
- Jung, T., S.K. Gulev, I. Rudeva, and V. Soloviov (2006), Sensitivity of extratropical cyclone characteristics to horizontal resolution in the ECMWF model, *Tech. Rep. 485*, Research Dept. ECMWF.
- Lambert, S., and J.C. Fyfe (2006), Changes in winter cyclone frequencies and strengths simulated in enhanced greenhouse gas experiments: Results from the models participating in the IPCC diagnostic exercise., *Climate Dynamics*, doi:10.1007/s00382-006-0110-3.

- Leckebusch, G.D., B. Koffi, U. Ulbrich, J.G. Pinto, T. Spangehl, and S. Zacharias (2006), Analysis of frequency and intensity of winterstorm events in Europe on synoptic and regional scales from a multi-model perspective, *Climate Research*, 31, 59–74.
- Pryor, S.C., J.T. Schoof, and R.J. Barthelmie (2005), Potential climate change impacts on wind speeds and wind energy density in northern Europe: Results from empirical downscaling of multiple AOGCMs, *Climate Research*, 29, 183–198.
- van den Brink, H.W., G.P. Können, and J.D. Opsteegh (2004), Statistics of extreme synoptic-scale wind speeds in ensemble simulations of current and future climate, *Journal of Climate*, 17, 4564–4574.
- van den Hurk et al, B.J.J.M. (2006), Integrating global and regional model results into new climate change scenarios for the Netherlands, *Nature*, *submitted*.
- van Ulden, A.P., and G.J. van Oldenborgh (2006), Large-scale atmospheric circulation biases and changes in global climate model simulations and their importance for climate change in Central Europe, *Atmos. Chem. Phys.*, 6, 863–881.
- Verkaik, J.W. (2000), Evaluation of two gustiness models for exposure correction calculations, *Journal of Applied Meteorology*, 39(9), 1613–1626.
- Yin, J.H. (2005), A consistent poleward shift of the storm tracks in simulations of 21st century climate, *Geophys. Res. Lett.*, 32, L18701, doi:10.1029/2005GL023684.

List of Figures

1	Global averaged temperature as derived from the ERA40 data and from the GCMs according to the SRESA1B scenario.	11
2	Winter-mean (O-M) MSLP for ERA40 (lines) and difference between model and ERA40 climatology (shaded). Units are in hPa.	12
3	Winter-mean (O-M) wind speed of ERA40 (lines) and absolute difference of GCM with ERA40 in winter-mean (O-M) wind speed (shaded). Units are in m/s for all panels.	13
4	Gumbel plots of the annual maximum wind speed for the grid points nearest to (3.2E;53.2N) for the PRUDENCE RCMs, as well as the ERA40 dataset, and the observational set for (3.2E;53.2N). The lines are the GEV-fits to the data; Note that the average fit of the RCMS coincides with the fit of the driving GCM	14
5	Cross section of the average annual minimum mean sea level pressure (left) and the annual maximum wind speed at 10m height (right) in the area 25W-10W and period 1960-1990. Shown are results from ERA40, the control run of HadAM3H, and two RACMO2 simulations driven by these GCM boundaries.	15
6	Winter-mean (O-M) MSLP for 20C3M (lines), and difference between SRESA1B and 20C3M (shaded). Units are hPa.	16
7	Annual minimum MSLP for 20C3M (lines), and difference between SRESA1B and 20C3M (shaded). Units are hPa.	17
8	Winter-mean (O-M) wind speed of 20C3M (lines) and relative difference (%) between SRESA1B and 20C3M winter-mean (O-M) wind speed (shaded).	18
9	20C3M (lines) winter-mean (O-M) wind speed (m/s) and relative difference (%) between SRESA1B and 20C3M annual maximum wind speeds (shaded).	19
10	Zonally averaged relative change in the annual wind speed maxima (left), and the zonally averaged absolute change in the annual MSLP minima (right) for different models. Compared are the 20C3M and the SRESA1B scenarios.	20
11	Return level plots of the annual extreme wind speed for the GCMs (open circle: 20C3M, closed circle: SRESA1B) and ERA40 (square). for the grid point nearest to (2.5 °E,55 °N). The lines are the fits to a Gumbel distribution.	21
12	Change in the annual maximum wind speed for the grid point nearest to (2.5°E,55°N), as a function of the global temperature change. Shown are the changes for 2046-2065, 2081-2100, 2181-2200 and 2281-2300 (if available) relative to the 1961-2000 20C3M period. Error-bars indicate estimated σ -levels.	22
13	Histogram of the change in the once-per-year exceeded wind speed for the area 0-10°E;50-60°N; the smooth line is a fitted spline function. The model results are linearly scaled to a global temperature increase of 2°. Right: models with large change in zonal flow; Left: model with small change in zonal flow.	23
14	Return level plot of the annual maxima of the wind speed and the annual minima of the MSLP, averaged over (30–70°N en -90–10°E) for the MPI-ECHAM5 model.	24

Figure 1: Global averaged temperature as derived from the ERA40 data and from the GCMs according to the SRESA1B scenario.

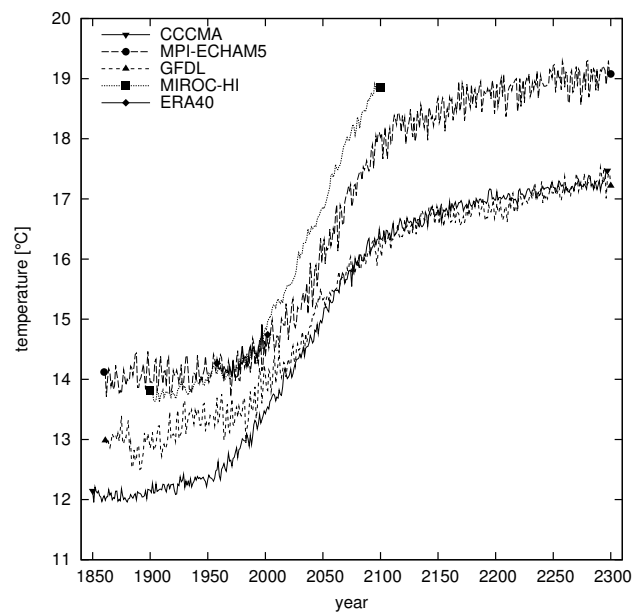


Figure 2: Winter-mean (O-M) MSLP for ERA40 (lines) and difference between model and ERA40 climatology (shaded). Units are in hPa.

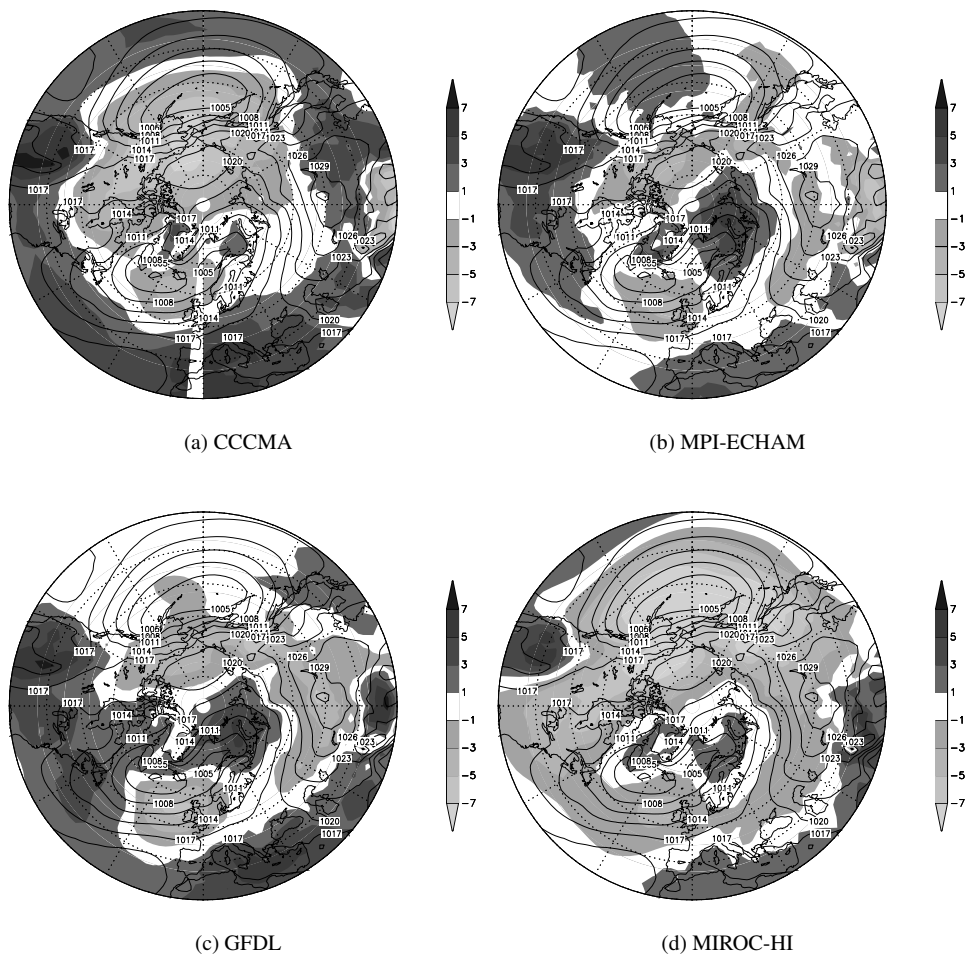


Figure 3: Winter-mean (O-M) wind speed of ERA40 (lines) and absolute difference of GCM with ERA40 in winter-mean (O-M) wind speed (shaded). Units are in m/s for all panels.

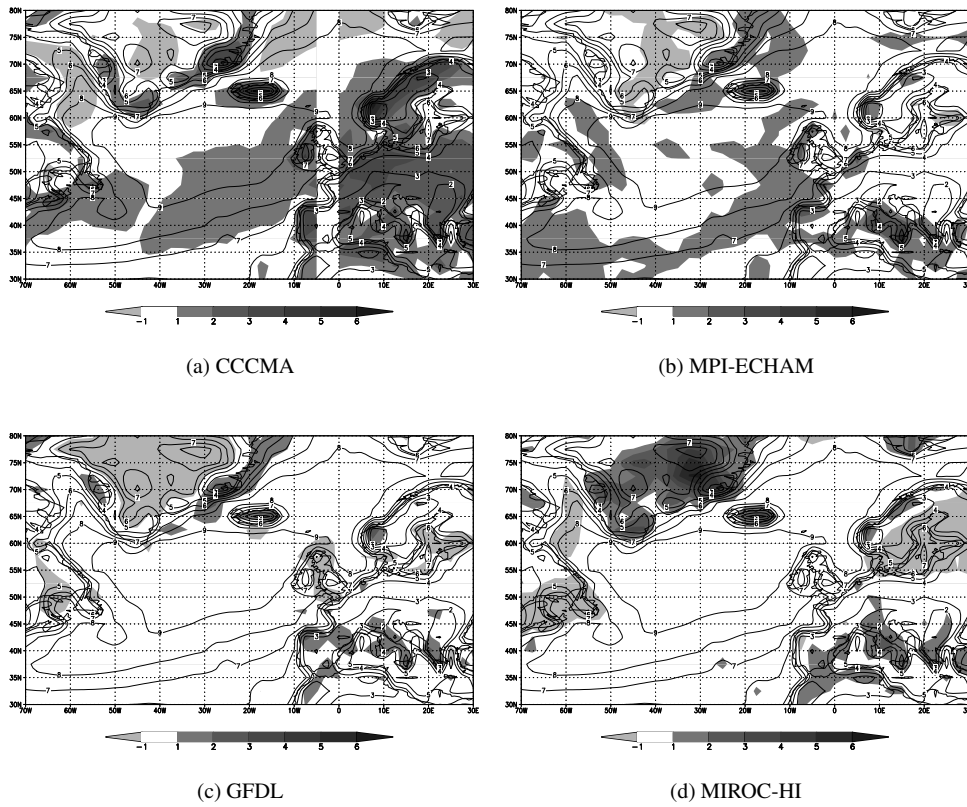


Figure 4: Gumbel plots of the annual maximum wind speed for the grid points nearest to (3.2E;53.2N) for the PRUDENCE RCMs, as well as the ERA40 dataset, and the observational set for (3.2E;53.2N). The lines are the GEV-fits to the data; Note that the average fit of the RCMS coincides with the fit of the driving GCM

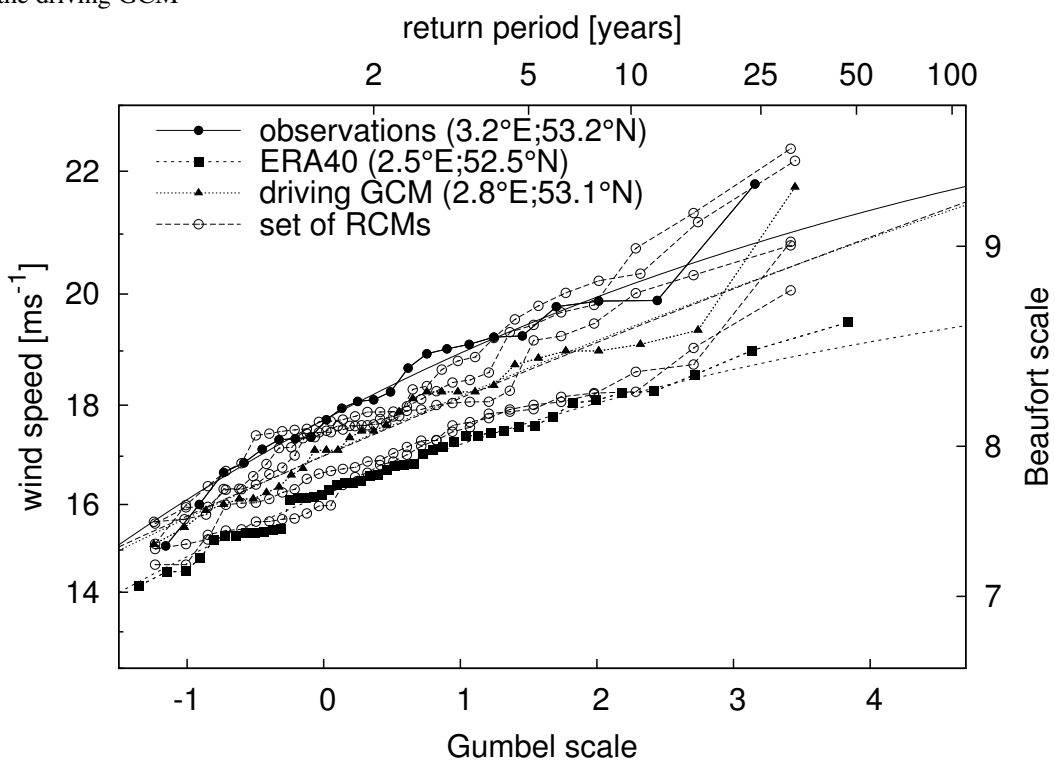


Figure 5: Cross section of the average annual minimum mean sea level pressure (left) and the annual maximum wind speed at 10m height (right) in the area 25W-10W and period 1960-1990. Shown are results from ERA40, the control run of HadAM3H, and two RACMO2 simulations driven by these GCM boundaries.

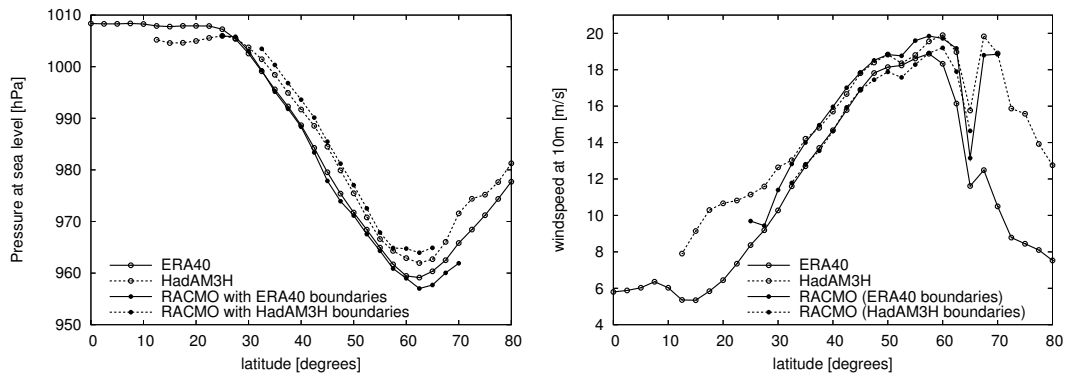


Figure 6: Winter-mean (O-M) MSLP for 20C3M (lines), and difference between SRESA1B and 20C3M (shaded). Units are hPa.

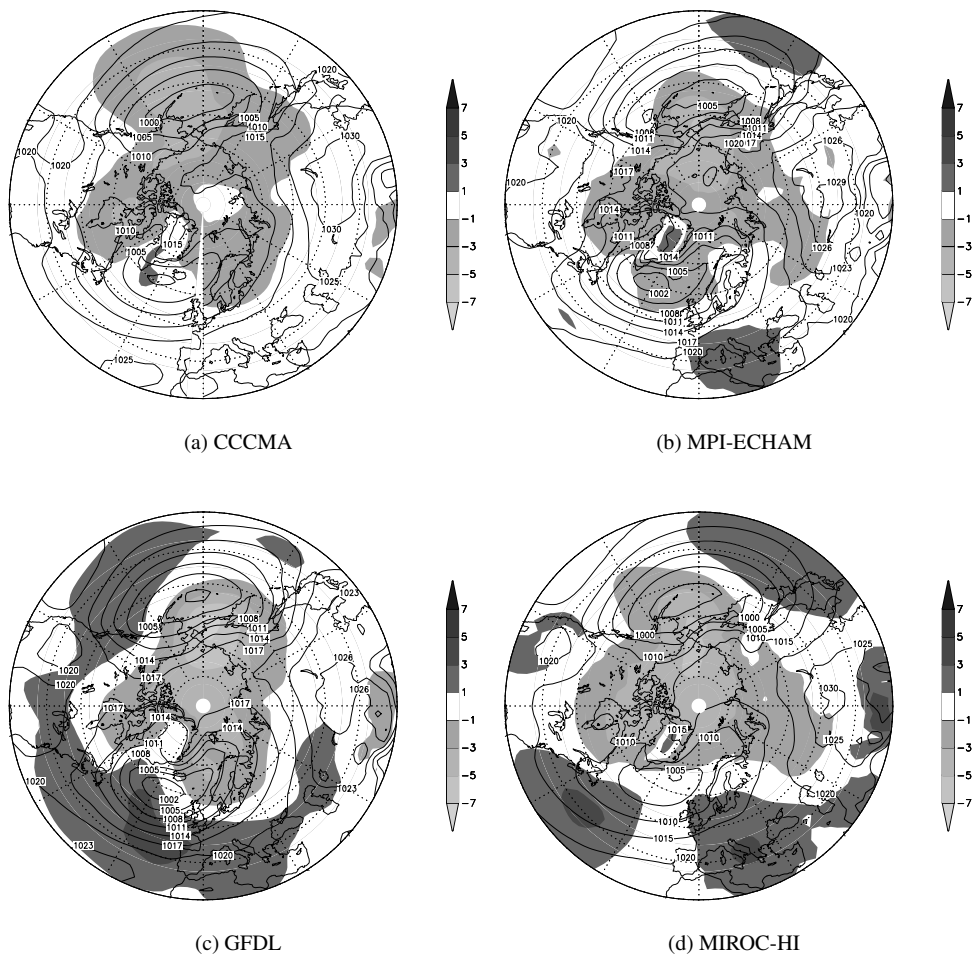


Figure 7: Annual minimum MSLP for 20C3M (lines), and difference between SRESA1B and 20C3M (shaded). Units are hPa.

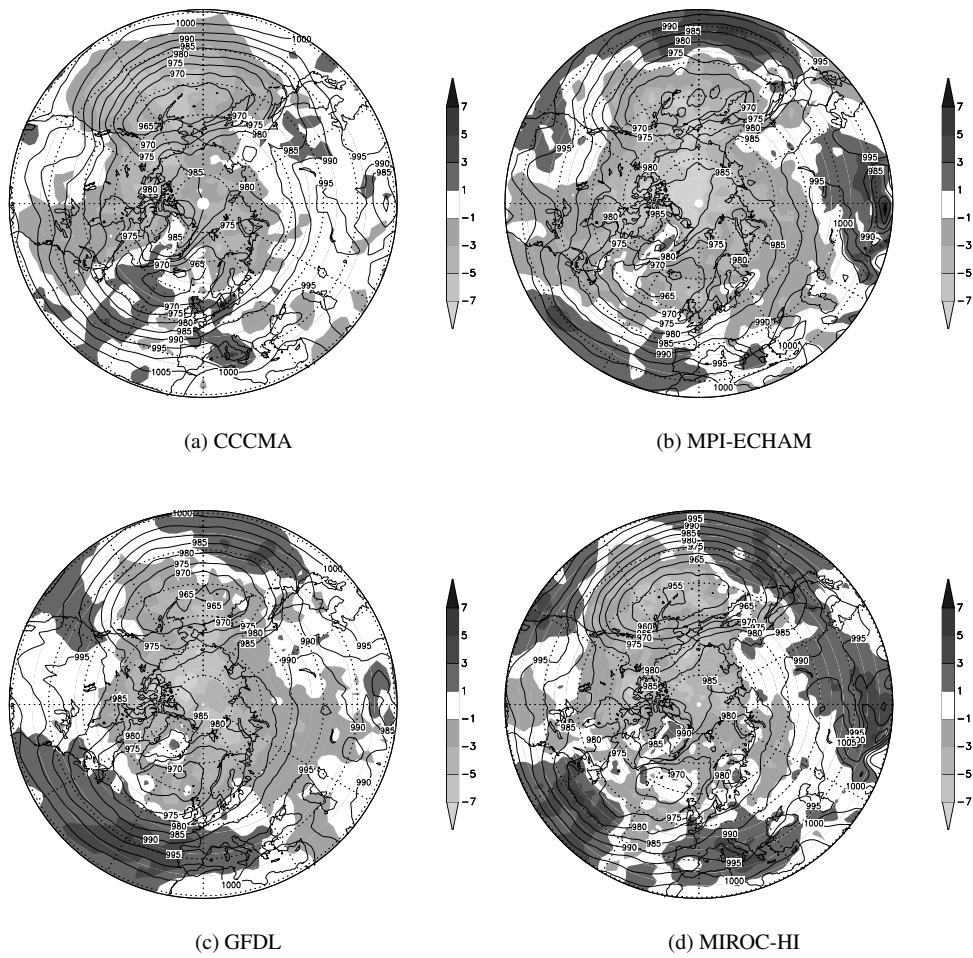


Figure 8: Winter-mean (O-M) wind speed of 20C3M (lines) and relative difference (%) between SRESA1B and 20C3M winter-mean (O-M) wind speed (shaded).

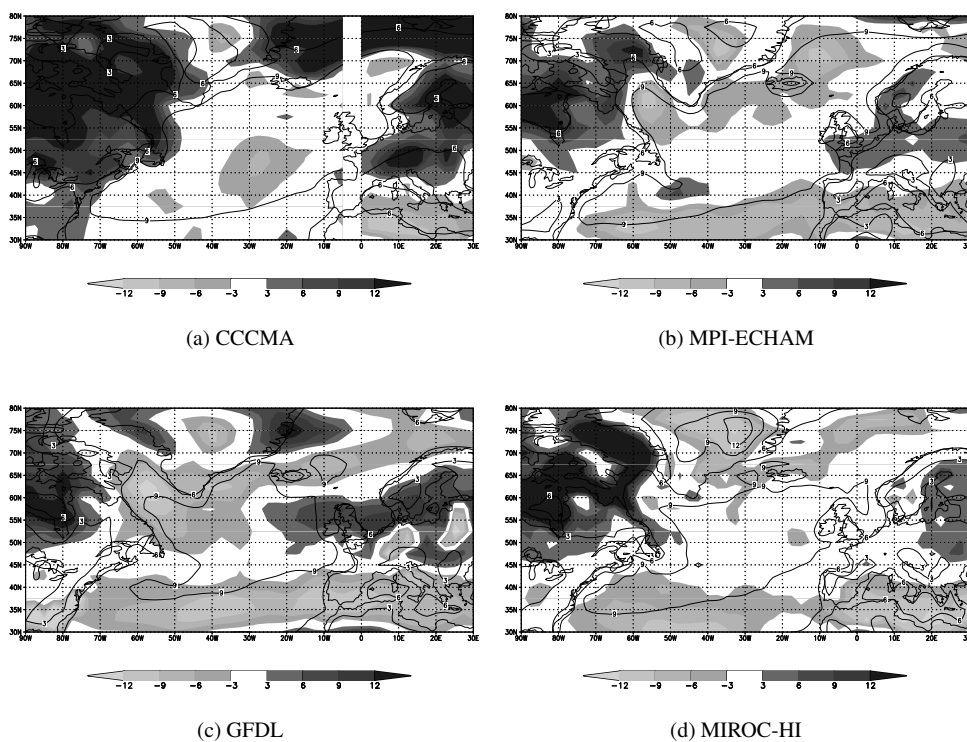


Figure 9: 20C3M (lines) winter-mean (O-M) wind speed (m/s) and relative difference (%) between SRESA1B and 20C3M annual maximum wind speeds (shaded).

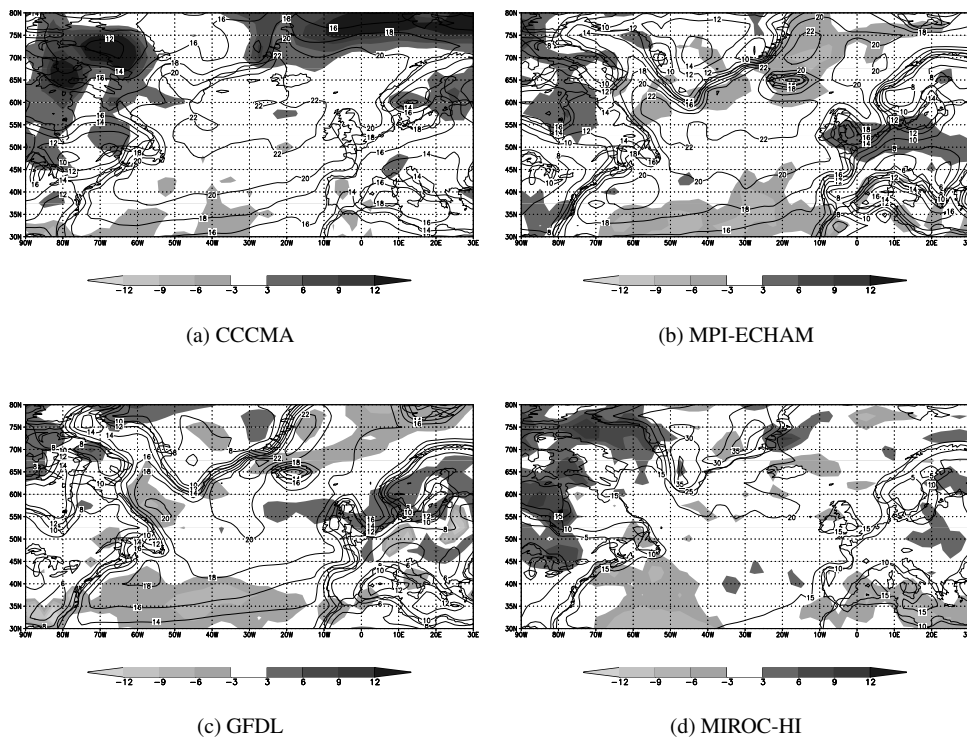


Figure 10: Zonally averaged relative change in the annual wind speed maxima (left), and the zonally averaged absolute change in the annual MSLP minima (right) for different models. Compared are the 20C3M and the SRESA1B scenarios.

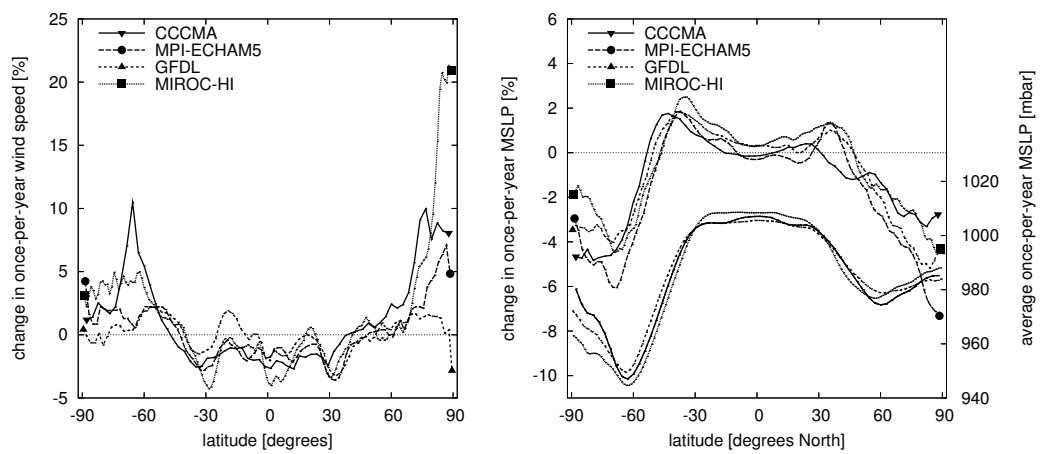


Figure 11: Return level plots of the annual extreme wind speed for the GCMs (open circle: 20C3M, closed circle: SRESA1B) and ERA40 (square). for the grid point nearest to (2.5 °E,55 °N). The lines are the fits to a Gumbel distribution.

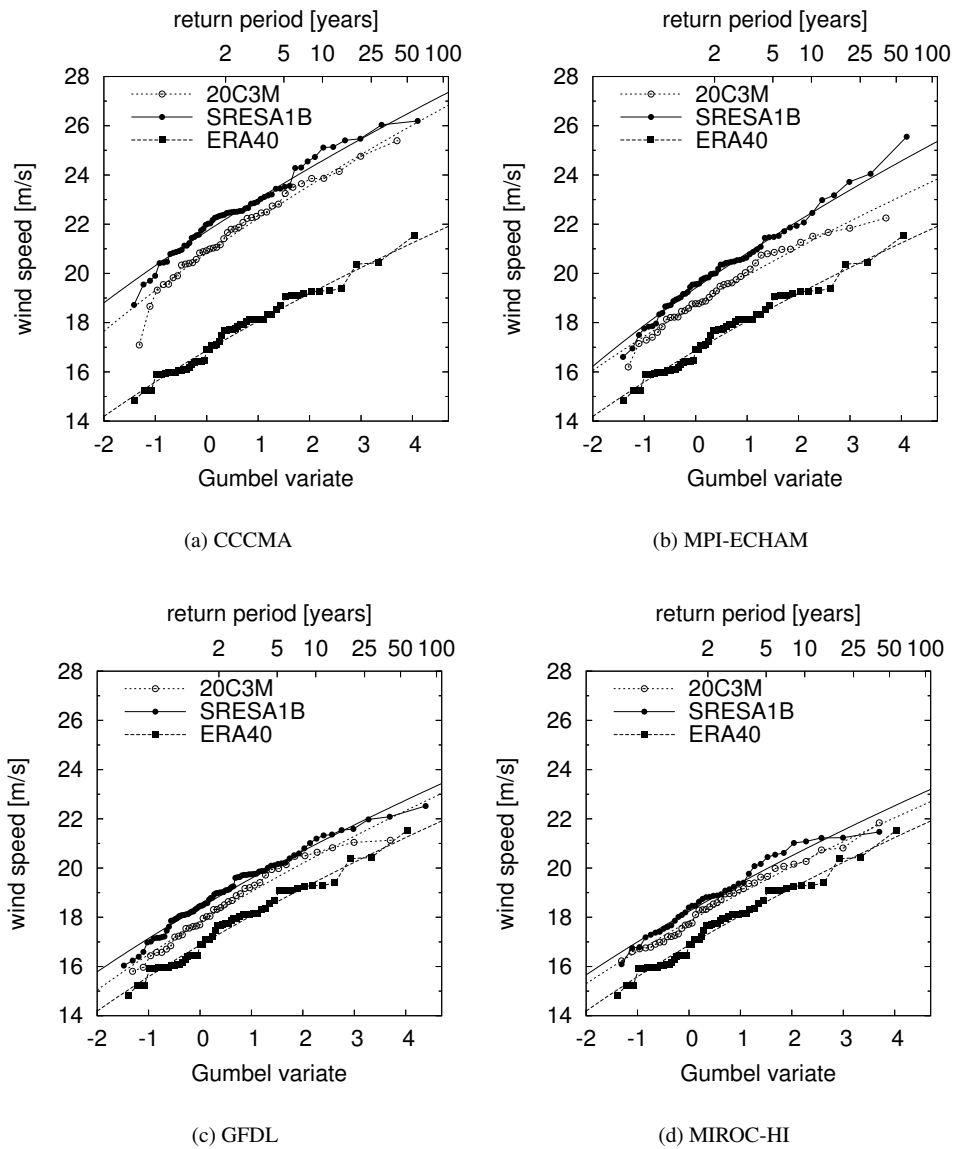


Figure 12: Change in the annual maximum wind speed for the grid point nearest to (2.5°E,55°N), as a function of the global temperature change. Shown are the changes for 2046-2065, 2081-2100, 2181-2200 and 2281-2300 (if available) relative to the 1961-2000 20C3M period. Error-bars indicate estimated σ -levels.

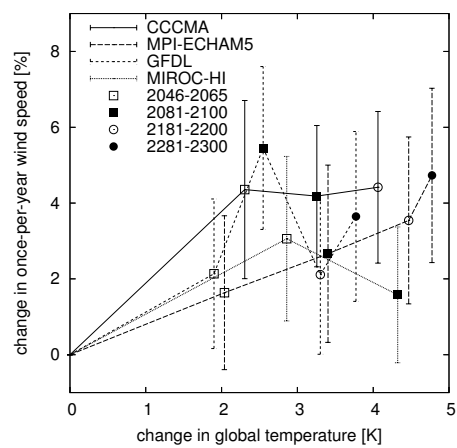


Figure 13: Histogram of the change in the once-per-year exceeded wind speed for the area 0-10°E;50-60°N; the smooth line is a fitted spline function. The model results are linearly scaled to a global temperature increase of 2°. Right: models with large change in zonal flow; Left: model with small change in zonal flow.

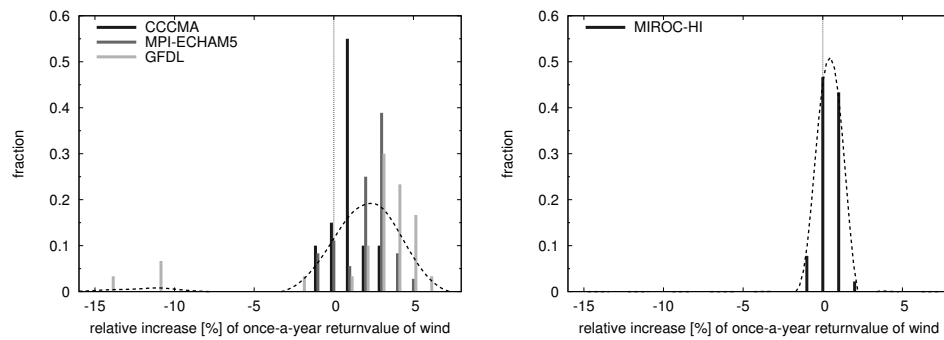
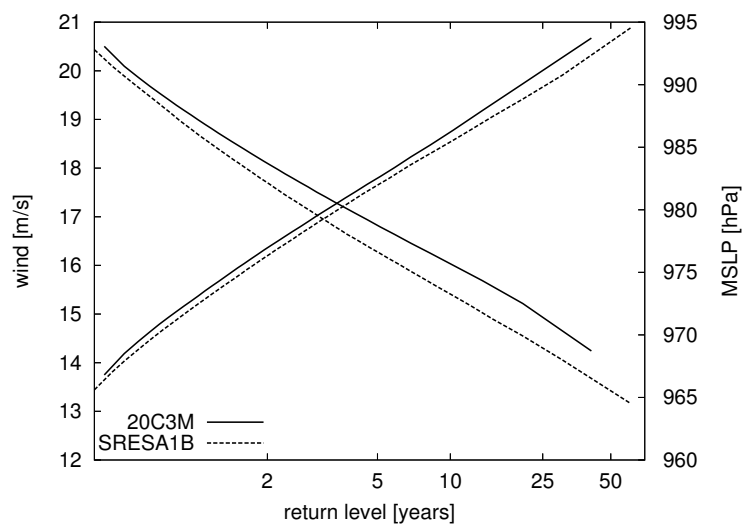


Figure 14: Return level plot of the annual maxima of the wind speed and the annual minima of the MSLP, averaged over (30–70°N en -90–10°E) for the MPI-ECHAM5 model.



List of Tables

1	Description of the models used in this study. See e.g. UvO, and their references, for a more comprehensive documentation.	26
2	Daily-mean data available via the PCMDI archive.	27

Table 1: Description of the models used in this study. See e.g. UvO, and their references, for a more comprehensive documentation.

Model name	full model name	resolution
CCCMA	CGCM3.1(T63)	T63,L31
MPI-ECHAM	ECHAM5/MPI-OM	T63,L31
GFDL	GFDL-CM2.1	2.5°×2.0°,L24
MIROC-HI	MIROC3.2(hires)	T106,L56

Table 2: Daily-mean data available via the PCMDI archive.

	20C3M	SRESA1B			
CCCMA	1960-2000	2046-2065	2081-2100	2181-2200	
MPI-ECHAM	1960-2000	2046-2065	2081-2100	2181-2200	2281-2300
GFDL	1960-2000	2046-2065	2081-2100	2181-2200	2281-2300
MIROC-HI	1960-2000	2046-2065	2081-2100		